Boiling regimes in a closed two-phase thermosyphon

A. NIRO

Dipartimento di Energetica, Politecnico di Milano, Milano 20133, Italy

and

G. P. BERETTA

Dipartimento di Ingegneria Meccanica, Università di Brescia, Brescia 25060, Italy,
and Department of Mechanical Engineering, MIT, Cambridge, MA 01239, U.S.A.

Abstract—Experimental results and an analytical model on the boiling mechanisms in a closed two-phase thermosyphon are presented in order to define the frontiers between the main boiling regimes and, in particular, the frontier between intermittent boiling and fully-developed boiling. The boiling regimes are classified on the basis of the frequency of bubble nucleation and the ratio of bubble diameter to device diameter. A criterion for the intermittent/developed-boiling frontier is based on the ratio of the bubble-nucleation waiting time and the bubble growth time. From this criterion a correlation between power throughput, working-fluid pressure and nucleation critical superheat are obtained. Experimental data on operating conditions, temperatures, and nucleation frequencies show the same functional dependence as the proposed correlation.

1. INTRODUCTION

THE PURPOSE of this work is to study experimentally and theoretically the boiling mechanisms in a closed two-phase thermosyphon for medium and large fillings, in order to define the frontiers between the main regimes and, in particular, the frontier between intermittent boiling and fully-developed boiling.

Closed two-phase thermosyphons (or wickless heat-pipes) can operate in two different ways depending on fluid filling: the 'falling film evaporation' mode for small fillings (liquid volume less than about 10% of the evaporator volume), and 'pool boiling' for medium and large fillings (from 30 to 100% and over of the evaporator volume). In the falling-film evaporation mode all the thermosyphon walls are wetted by a continuous liquid film which, however, for most fluids is stable only at very low thermal fluxes. In the pool-boiling mode, instead, the thermosyphon evaporator is flooded, boiling is sustained over a wide range of operating fluids and conditions, and the power throughput is much greater. Therefore, pool boiling is the mode of operation of technological interest. However, there are many boiling regimes characterized by different degrees of steadiness, which affect differently the thermosyphon performance.

In the last 15 years the fluid dynamic phenomena related to mass, momentum and heat transfer between evaporator and condenser have been extensively studied in order to determine the operating limits; Imura *et al.* [1] reviewed about ten different relations for the flooding limit. The boiling phenomena in the evaporator have almost always been overlooked, even in some new theoretical models [2, 3], although instabilities and unsteady regimes have been known for a long time [4–6] to depend on the details of the boiling mechanisms. Casarosa *et al.* [7] clearly showed experimentally the existence of strongly intermittent boiling regimes.

To optimize the performance of a closed two-phase thermosyphon, the designer must avoid such regimes and, therefore, be aware of the causes of the unsteady behavior. Unsteady regimes cause large-amplitude oscillations in many characteristic variables, such as the evaporator wall temperature that can exceed the design values. Moreover, for evaporator fixed-temperature boundary conditions, the operation may result blocked when not expected. However, no correlations for the frontier between intermittent and fully-developed boiling are available in the literature.

In this paper, we first review the boiling regimes and the causes of unsteady operation; then, we propose criteria for classifying the main regimes and obtain analytical correlations for the intermittent/fully-developed-boiling frontier and slug/bubble-boiling frontier; finally, we discuss the experimental results and a diagram where the frontiers are plotted.

2. BOILING REGIMES

If the thermosyphon is initially isolated, the liquid is at rest in the evaporator and is in thermodynamic equilibrium with its vapor that fills the remaining volume of the device. The temperature is imposed by the heat sink, in contact with the thermosyphon

NOMENCLATURE

a liquid thermal diffusivity, $k_f/\rho_f c_f$

b thermal boundary layer thickness

$c_1, c_{0.75}, c_m$ bubble growth constants

c_3, c'_3 coefficients of inertia and friction effects terms, $c_3 = 0.1875c'_3 = 0.1875(1.330+0.5c_w)$

c_f liquid specific heat

c_w coefficient of friction effects term

D device diameter

D_d bubble diameter at detachment

D_{d_1} bubble diameter at detachment in the dynamic limit

D_{d_2} bubble diameter at detachment in the static limit

f nucleation frequency, $1/(\tau_w+\tau_g)$

h_{fg} vaporization enthalpy

G constant defined by equation (23), $(\sqrt{\pi}(gk_f)^{1/3}(\rho_f c_f)^{5/12}\Delta p^{*0.75}/2(c_{0.75}c_3)^{1/3})$

Ja Jakob number, $\rho_f c_f \theta/\rho_g h_{fg}$

$\tilde{Ja}$ Jakob number for which liquid inertia balances adhesion forces in the bubble growth

$\overline{Ja}$ Jakob number for which q_{wg_1} is equal to q_{wg_2}

k_f liquid thermal conductivity

p_{dist} liquid pressure fluctuation

p_f liquid pressure

p_g vapor pressure

$p_{g,ads}$ pressure of gas or vapor entrapped in a cavity

p_r reduced pressure

p_s saturation pressure

p' derivative of saturation pressure with respect to temperature, dp_s/dT

Δp^* critical pressure difference at bubble interface

q thermal flux

q_{wg} thermal flux at intermittent/fully-developed frontier

q_{wg_1} thermal flux at intermittent/fully-developed frontier in the dynamic limit

q_{wg_2} thermal flux at intermittent/fully-developed frontier in the static limit

r radial coordinate

R bubble radius

R_c mouth cavity radius

R_s contact area radius between bubble and surface

T_g vapor temperature

T_{f_x} uniformly superheated liquid temperature

$T_s(p_f)$ saturation temperature for $p = p_f$

x distance from heated wall

z axial coordinate.

Greek symbols

ε ratio of bubble diameter to device diameter, D_d/D

$\theta(r, z, t)$ liquid superheat

$\theta_w(x, z, t)$ liquid superheat near the wall

θ^* critical liquid superheat

ρ_f liquid density

ρ_g vapor density

σ surface tension

τ_g bubble growth time

τ_{g_1} bubble growth time for the dynamic limit

τ_{g_2} bubble growth time for the static limit

τ_w nucleation waiting time

Φ contact angle between bubble and heated surface.

through the condenser. At time t_0 we begin to power the heat source, the liquid starts to superheat. Evaporation begins from the free surface. Boiling, instead, starts when the liquid reaches a critical superheat, i.e. a critical value of temperature greater than the saturation temperature corresponding to the pressure in the device. The critical superheat for bubble nucleation depends on the heated surface characteristics (roughness, adsorbed gases or vapors) and the thermodynamic properties of the fluid (vapor density and enthalpy of vaporization).

Depending on the extent of the critical liquid superheat, boiling may be characterized by a broad spectrum of nucleation frequencies and bubble dimensions. The nucleation frequencies can range from less than 0.01 Hz to more than 50 Hz. Low nucleation frequencies (<0.1 Hz) bring about the intermittent-boiling regime: long periods of liquid quietness (up to several hundreds of seconds) alternate with sudden and almost explosive vapor nucleations; the nucleation is generally followed by strong boiling that quickly goes out giving way to a new period of quietness. Low nucleation frequencies are related in fact to high liquid superheats that cause the formation of large bubbles with respect to the device diameter. Obviously, the lower the nucleation frequency, the more uneven and unsteady becomes the operation of the thermosyphon. High nucleation frequencies (> 10 Hz) bring about the fully-developed boiling: thick jets of small bubbles (1–2 mm diameter) detach from one or more active cavities on the heated surface, making the fluid strongly turbulent in the evaporator. For frequencies between 0.1 and 10 Hz we have transition regimes characterized by intermediate bubble growth rates and bubble dimensions. A particular transition regime is the slug-developed boiling,

characterized by nucleation frequencies of about 1 Hz, bubble dimensions comparable with the device diameter, and a slow formation of vapor slugs. In accordance with these observations, we classify the different regimes based on the nucleation frequency and the ratio of bubble diameter to device diameter.

The boiling process consists of the sequence of the processes of bubble nucleation, growth and detachment. Experimentally we observed that nucleation in our thermosyphons always occurs at the wall. This is because the heated surface has some roughness, cavities and scratches of various sizes that become active if some gas or vapor is entrapped. In a uniformly superheated liquid, nucleation occurs at an active cavity when the liquid reaches the critical superheat

$$\theta^* \approx \frac{1}{dp_s/dT} \Delta p^* \tag{1}$$

where Δp^* is the difference between vapor pressure and liquid pressure when the nucleus reaches the critical dimensions. From equation (1) we see that for a given Δp^* the lower dp_s/dT the higher the critical superheat. For example, for water dp_s/dT decreases by a factor of 50 between 120 and 20°C and, therefore, the superheats needed for nucleation at 20°C are 50 times higher than at 120°C. Thus, the critical superheat θ^* is a function of the pressure p (since dp_s/dT is a monotonic function of p_s) and increases as pressure decreases. Because the hypothesis of uniform liquid superheat is not actually verified, we further assume (as suggested by Hsu [8]) that the critical superheat θ^* is reached by a liquid layer of thickness b near the heated wall. For b we assume the value $1.5R_c$ proposed by Han and Griffith [9].

We define the waiting time τ_w as the time needed to attain the critical superheat θ^* in the layer of thickness b. The waiting time ends and the growth time τ_g begins when the vapor nucleus, after reaching the critical dimension, starts to grow quickly. The growth time ends when the bubble detaches from the heated surface. The inverse of the period of a whole cycle, i.e. of the sum of the waiting time and the growth time is defined by Han and Griffith [9] as the nucleation frequency

$$f = \frac{1}{\tau_w + \tau_g}. \tag{2}$$

For τ_w much longer than τ_g, the nucleation frequency obviously coincides with the inverse of the waiting time.

3. INTERMITTENT VS FULLY-DEVELOPED-BOILING FRONTIER

We say that boiling is 'fully developed' when the waiting time τ_w is much shorter than the growth time τ_g, whereas boiling is 'intermittent' when the waiting time τ_w is much longer than the growth time τ_g. Thus,

the transition frontier between the intermittent-boiling regime and the fully-developed-boiling regime is determined by the criterion

$$\tau_w \sim \tau_g. \tag{3}$$

In order to derive from criterion (3) a relation between fluid thermodynamic properties, geometric characteristics and system boundary conditions, we need to estimate τ_w and τ_g.

3.1. Determination of τ_w

The waiting time τ_w can be determined by the general nucleation criterion

$$\theta(R-b, z_s, \tau_w) = \theta^* \tag{4}$$

where $\theta(r, z, t)$ describes in cylindrical coordinates the liquid superheat as a function of the distance r from the evaporator axis, the height z_s in the evaporator of the nucleation site, and time t. The liquid superheat near the heated surface is determined by three contributions: (a) the thermal boundary layer; (b) the bulk heating of the liquid in the evaporator; and (c) the cooling of the vapor in the condenser which reduces the vapor temperature and, hence, the saturation pressure and temperature. However, the characteristic times of the three superheat contributions are quite different: the boundary-layer characteristic time is of the order of 0.1 s and is much shorter than the characteristic times of the other two contributions (b) and (c) which are of the order of 10 s as reported in ref. [10]. Since the bubble growth time τ_g is always shorter than 200 ms and, by virtue of criterion (3), the waiting time τ_w at the transition frontier is of the same order of magnitude as τ_g, we can consider only the thermal boundary layer contribution θ_w and neglect the other two contributions. We express θ_w more conveniently in Cartesian coordinates, i.e. $\theta_w = \theta_w(x, z, t)$ where x is the distance from the heated wall. We have observed experimentally that liquid mixing due to boiling is equally effective at all heights in the evaporator at the transition frontier. Hence, we assume that the heat transfer coefficient and therefore the liquid superheat at the wall θ_w, for fixed thermal flux boundary conditions, depend weakly on height z. Equation (4) becomes

$$\theta_w(b, \tau_w) = \theta^*. \tag{5}$$

Finally because the convection intensity near the solid wall is dumped down due to the no-slip boundary condition, we may assume as suggested by Han and Griffith [9] a purely conductive heat transfer mechanism in the liquid near to the heated wall. Accordingly, the waiting time may be approximated by

$$\tau_w = \frac{\pi}{4} \left(1 + \frac{bq}{k_f \theta^*} \right)^2 k_f \rho_f c_f \frac{\theta^{*2}}{q^2} \tag{6}$$

obtained by linearizing the pure conduction solution for a semiinfinite geometry and fixed thermal flux boundary conditions.

3.2. Determination of τ_g

To determine the growth time we need the bubble growth law and the force balance that controls bubble detachment from the heated surface. At the detachment instant, the force balance is

$$F_b = F_s + F_{li} + F_f \qquad (7)$$

i.e. buoyancy (F_b) balances surface adhesion forces (F_s), liquid inertia (F_{li}) and viscous drag (F_f). We observed experimentally (with a high speed camera) that the shape of the growing bubble is nearly spherical (also for high superheat). Thus, the balance (7) may be written as

$$\tfrac{4}{3}\pi R^3 \rho_f g = 2\pi\sigma R_s \sin\Phi + \tfrac{4}{3}\pi R^2 \dot{R}^2 \rho_f + \frac{c_w}{2}\pi R^2 \dot{R}^2 \rho_f$$

$$(8)$$

where R_s is the contact radius between bubble and surface (assumed to be constant and independent of the bubble radius R), $\dot{R}$ the bubble detachment velocity (the bubble is assumed to be tangent to the heated surface), c_w an empirical drag coefficient, as reported in refs. [11, 12], since the friction forces are not sufficiently known. The angle Φ should be the contact angle between bubble and heated surface for a horizontal surface. Here we assume that Φ includes also a geometry factor, taking into account that our surface is vertical. The inertia term is derived from the Witze et al. [13] solution, obtained for a spherical bubble growing tangent to the surface in semiinfinite liquid and for inviscid and irrotational flow. The assumption of semiinfinite liquid implies that balance (8) holds only for small bubbles with respect to the device diameter. This assumption is further discussed later. Inertia forces and viscous forces have the same functional dependence from R and $\dot{R}$, and may be grouped in a single term $c_3' \pi R^2 \dot{R}^2 \rho_f$, where $c_3' = (1.333 + 0.5c_w)$.

Determining the bubble growth law as a function of liquid superheat and thermodynamic properties is a hard problem. For small superheats and a pressure not much lower than atmospheric, the growth is wholly controlled by the heat transfer mechanisms (negligible liquid inertia). In the limit of negligible inertia we find the so-called 'asymptotic solution'

$$R = c_1 Ja\sqrt{(at)} \qquad (9')$$

where Ja is the Jakob number, $Ja = \rho_f c_f \theta / \rho_g h_{fg}$, and a the liquid diffusivity, $a = k_f / \rho_f c_f$. The range of validity of equation (9') is discussed in the Appendix.

When the inertia effects are not negligible, equation (9') ceases to hold and the bubble growth law becomes complex [14–16]. Since we need an analytical expression, we use the empirical growth equation proposed by Cole and Shulman [17]

$$R = c_{0.75} Ja^{0.75}\sqrt{(at)}. \qquad (9'')$$

The range of validity for equation (9'') is also discussed in the Appendix. Both equations (9') and (9'') can be

written in the form

$$R = c_m Ja^m \sqrt{(at)}. \qquad (10)$$

Using equation (10) in balance (8), we obtain the growth time

$$\tau_g = \left(c_m c_3 \left(\frac{a}{g^2}\right)^{1/2} Ja^m + \frac{3\sigma R_s \sin\Phi}{2\rho_f g c_m^3 Ja^{3m} a^{1.5}} \right)^{2/3} \qquad (11)$$

where $c_3 = 0.1875 c_3'$. The first term within parentheses is the ratio between dynamical forces (liquid inertia and viscous drag) and buoyancy; the second term is the ratio between surface adhesion force and buoyancy. Equation (11) has two interesting limit solutions

$$\tau_{g_1} = (c_m c_3)^{2/3} \left(\frac{a}{g^2}\right)^{1/3} Ja^{(2/3)m} \qquad (12)$$

$$\tau_{g_2} = \left(\frac{3\sigma R_s \sin\Phi}{2\rho_f g}\right)^{2/3} \frac{1}{c_m^2 Ja^{2m} a}. \qquad (13)$$

Equation (12), called the dynamic limit solution, holds when liquid inertia prevails over adhesion forces, i.e. when

$$c_m c_3 Ja^m \left(\frac{a}{g^2}\right)^{1/2} \gg \frac{3\sigma R_s \sin\Phi}{2\rho_f g c_m^3 Ja^{3m} a^{1.5}}$$

or, equivalently

$$Ja \gg \left(\frac{3\sigma R_s \sin\Phi}{2\rho_f g} \frac{1}{c_m^4 c_3} \frac{g}{a^2}\right)^{1/4m} = \widetilde{Ja}. \qquad (14')$$

Equation (13), called the static limit solution, holds when adhesion forces prevail over liquid inertia, i.e. when

$$Ja \ll \widetilde{Ja}. \qquad (14'')$$

3.3. Intermittent/fully-developed-boiling frontier correlation

Substituting relations (6) and (11) in criterion (3), and assuming that the term $(bq/k_f\theta^*)$ in equation (6) is negligible, we find the equation

$$q_{wg} = \frac{\sqrt{(\pi k_f \rho_f c_f)}}{2}$$

$$\times \frac{\theta^*}{\left(c_m c_3 \left(\frac{a}{g^2}\right)^{1/2} Ja^m + \frac{3\sigma R_s \sin\Phi}{2\rho_f g c_m^3 Ja^{3m} a^{1.5}} \right)^{1/3}} \qquad (15)$$

that gives the thermal flux q_{wg} at the transition frontier between intermittent boiling and fully-developed boiling, as a function of critical liquid superheat θ^* (and, therefore, of pressure p) and fluid thermodynamic properties. We see that boiling is 'fully developed', i.e. $\tau_w \ll \tau_g$, when $q \gg q_{wg}$.

In the dynamic limit ($Ja \gg \widetilde{Ja}$) and the static limit ($Ja \ll \widetilde{Ja}$), equation (15) can be simplified, respectively, to yield

$$q_{wg_1} = \frac{\sqrt{\pi}}{2(c_{0.75}c_3)^{1/3}}(gk_f)^{1/3}(\rho_f c_f)^{5/12}\frac{\Delta p^{*0.75}T^{0.25}}{\sqrt{p'}}$$

(16)

$$q_{wg_2} = \frac{\sqrt{\pi}}{2}c_1 k_f \rho_f c_f \left(\frac{2\rho_f g}{3\sigma R_s \sin \Phi}\right)^{1/3}\frac{\Delta p^{*2}}{p'^3 T}$$ (17)

where T is the saturation temperature corresponding to the pressure of the liquid, i.e. $T \equiv T_s(p_f)$, and p' denotes $(dp_s/dT)_{T = T_s(p_f)}$. Equations (16) and (17) are obtained using, respectively, equations (9") and (9'), and the equation

$$Ja = \frac{\rho_f c_f}{\rho_g h_{fg}}\theta = \frac{\rho_f c_f}{p'^2 T}\Delta p$$ (18)

derived by replacing in the Jakob number equation (1) ($\theta \approx \Delta p/p'$) and the Clausius–Clapeyron equation ($dp_s/dT = p' \approx \rho_g h_{fg}/T$).

It is interesting to point out that at the transition frontier the functional dependence of the thermal flux q_{wg} on the critical superheat $\theta^* \approx (\Delta p^*/p') \sim 1/p'$ ranges from $q_{wg} \sim \theta^{*0.5}$ to $q_{wg} \sim \theta^{*3}$ depending on whether the bubble growth is dominated by dynamic forces or static forces. If dynamic forces dominate, bubbles are not frequent and not small enough to yield bubble-fully-developed boiling; thus the functional dependence of q_{wg} on θ^* is not what we have in bubble-fully-developed boiling.

4. SLUG VS BUBBLE-BOILING FRONTIER

The regimes are characterized not only by the nucleation frequency $f = 1/(\tau_w + \tau_g)$, but also by the bubble dimensions D_d with respect to the device diameter D. For the same nucleation frequency and bubble dimension we may have different regimes depending on the device diameter, according to the three criteria

$$D_d/D \ll 1, \quad D_d/D \sim 1, \quad D_d/D \gg 1. \quad (19)$$

The criterion $D_d/D \ll 1$ identifies bubbles that are very small; the criterion $D_d/D \sim 1$ identifies bubbles with dimensions that are comparable with the device diameter (slugs); and the criterion $D_d/D \gg 1$ identifies very large bubbles (long slugs).

In order to derive from criteria (19) analytical relations, we need to estimate D_d. Substituting equations (11)–(13) in the growth law equation (10), we get the bubble diameter at detachment D_d, respectively, for the general case and the two limit solutions (dynamic and static), i.e.

$$D_d = 2\left(c_m^4 c_3\left(\frac{a^2}{g}\right)Ja^{4m} + \frac{3\sigma R_s \sin \Phi}{2\rho_f g}\right)^{1/3}$$ (20)

$$D_{d_1} = 2c_m^{4/3}c_3^{1/3}\left(\frac{a^2}{g}\right)^{1/3}Ja^{(4/3)m} \quad Ja \gg \tilde{Ja} \quad (20')$$

$$D_{d_2} = 2\left(\frac{3\sigma R_s \sin \Phi}{2\rho_f g}\right)^{1/3} \quad Ja \ll \tilde{Ja}. \quad (20'')$$

For $R_s = 0.5D_{d_2}\sin \Phi$, equation (20") becomes the known Fritz–Hende equation. Substituting equation (20) in the ratio $D_d/D = \varepsilon$, we find the equation

$$Ja_\varepsilon = \left(\frac{\varepsilon^3 D^3 - R_{d_2}^3}{8c_m^4 c_3(a^2/g)}\right)^{1/4m}$$ (21)

or, equivalently

$$p'^2 T = \frac{\rho_f c_f}{Ja_\varepsilon}\Delta p^* = \left(\frac{8c_m^4 c_3(a^2/g)}{\varepsilon^3 D^3 - R_{d_2}^3}\right)^{1/4m}\rho_f c_f \Delta p^*$$ (22)

obtained by replacing equation (18) in equation (21). For $\varepsilon = 1$ equation (22) gives the operating pressure p (that is a monotonic function of p' and T) at the transition frontier between slug boiling and bubble boiling as a function of fluid thermodynamic properties.

We say that boiling is bubble-fully-developed when equation (22) is verified for $\varepsilon \ll 1$ with $q \gg q_{wg}$ (where q_{wg} is given by equation (15)). The boiling is slug-fully-developed when equation (22) is verified for $\varepsilon \sim 1$ with $q \gg q_{wg}$; whereas it is slug-developed if equation (22) is verified for $\varepsilon \sim 1$ with $q \sim q_{wg}$. Finally, for $\varepsilon = D_d/D \gg 1$ equation (22) is not verified with $q \geq q_{wg}$ but only with $q < q_{wg}$ and, therefore, corresponds to a low-frequency boiling regime.

It is noteworthy that the use of equation (20) in the criteria $D_d/D \sim 1$ and $D_d/D \gg 1$ and, therefore, the use of equation (22) for $\varepsilon \geq 1$, would yield only qualitative results because equation (20) implies the assumption $D_d/D \ll 1$.

5. EXPERIMENTAL RESULTS

The aim of the experimental study was to gather information about the boiling regimes and the transition frontier between intermittent boiling and fully-developed boiling. To this end, we studied the trend of nucleation frequencies as a function of pressure and power throughput.

The experimental results were obtained with a specifically designed facility equipped with transparent pipes of 12 and 30 mm i.d. and 1000 mm long. The evaporator, adiabatic section and condenser were respectively 200, 400 and 400 mm long. The evaporator was electrically heated by a nickel–chrome ribbon externally wound around it. Liquid and vapor temperatures were measured by thermocouples directly exposed to the fluid and placed respectively at 50 mm from the evaporator bottom and 300 mm from the condenser top. The input and output power and the fluid pressure were also measured. Errors on temperature measurements were less than 0.1°C. Errors on measurements of input power, output power and pressure were respectively 15, 5 and 0.5%. The relatively high error on the input power measurement is due to the lack of thermal insulation around
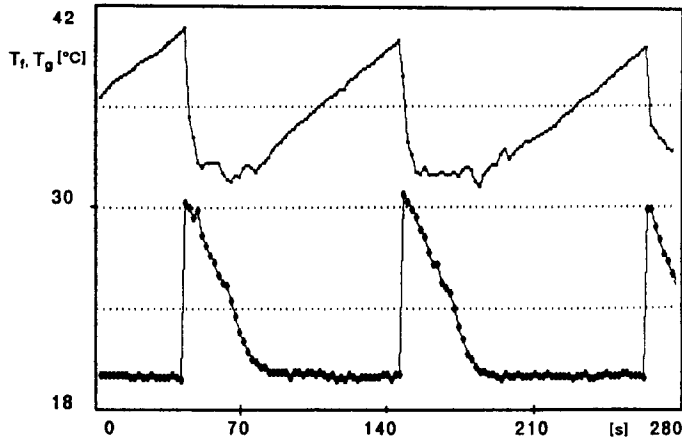
Fig. 1. Liquid and vapor temperature in a low-frequency boiling regime. $D = 12$ mm; fluid, water; $p_r = 10^{-4}$ and $\dot{Q} = 13$ W.

the evaporator. All measures were sampled automatically by an on-line computer at a maximum rate of 10 Hz. A video-recording of the thermosyphon operation was also performed by a video-camera and a stroboscope (the camera recording frequency was 50 Hz, but each frame was exposed for only 10 μs).

The thermosyphons were operated vertically. Most tests were run with water as the working fluid, some were run with acetone. The liquid filling corresponds to 80% of the evaporator volume. To span the transition between intermittent and fully-developed boiling, the operating conditions were varied so that the fluid pressure, expressed as reduced pressure, ranged between 10^{-4} and 10^{-2}. The tests were grouped in sequences carried out by changing the power throughput while holding the pressure at a fixed constant value different for every sequence.

A typical trend of liquid temperature (higher graph) and vapor temperature (lower graph) in a low-frequency boiling regime (about 0.01 Hz) is shown in Fig. 1, where the waiting phase and the boiling phase can be clearly recognized. During the waiting phase,

evaporator and condenser are weakly coupled. The liquid at rest in the evaporator is superheating, and the vapor in the condenser is cooling. The liquid temperature at the bottom of the evaporator rises almost linearly, whereas the vapor temperature in the condenser falls almost exponentially, as shown by Fig. 2, with a measured characteristic time of about 10 s, approaching the condenser wall temperature. When the critical superheat is achieved, vapor nucleation occurs. Due to the high available superheat, the bubble growth rate and its dimensions are so large that the liquid above the nucleation site is suddenly and violently ejected into the condenser. This causes a sharp rise of the condenser temperature and a corresponding fall of the liquid temperature. The final vapor temperature is lower than the measured liquid temperature because this is measured at the bottom of the evaporator where it is higher due to stratification built up during the waiting time. The liquid temperature decreases due to mixing of the liquid remaining in the evaporator with the cooled liquid returning from the condenser. After the first burst,
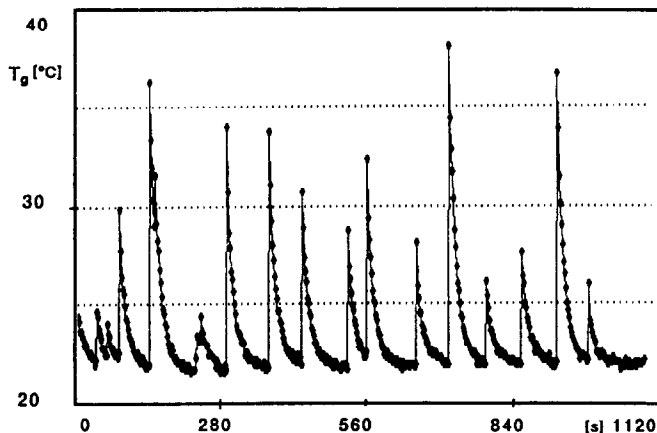

Fig. 2. Liquid and vapor temperature in a low-frequency boiling regime. $D = 12$ mm; fluid, water; $p_r = 10^{-4}$ and $\dot{Q} = 32$ W.

nucleation continues with decreasing intensity, stimulated by pressure perturbations. As the pressure perturbations weaken, boiling dies out and a new waiting phase begins. The dynamically controlled nucleation, in fact, unlike thermally controlled nucleation is not stable. The pressure in the thermosyphon always remains very close to the saturation pressure corresponding to the temperature of the vapor.

As the power throughput is increased, the critical superheat is attained in a shorter time and the waiting time between two successive bursts decreases, i.e. the burst frequency increases. As the burst frequency increases, non-linear phenomena such as pressure perturbations appear. These phenomena favor the nucleation and cooperate to further increasing the average nucleation frequency. The sequence shown in Figs. 3(a)–(d) are examples of transition between low-frequency boiling and fully-developed boiling. The
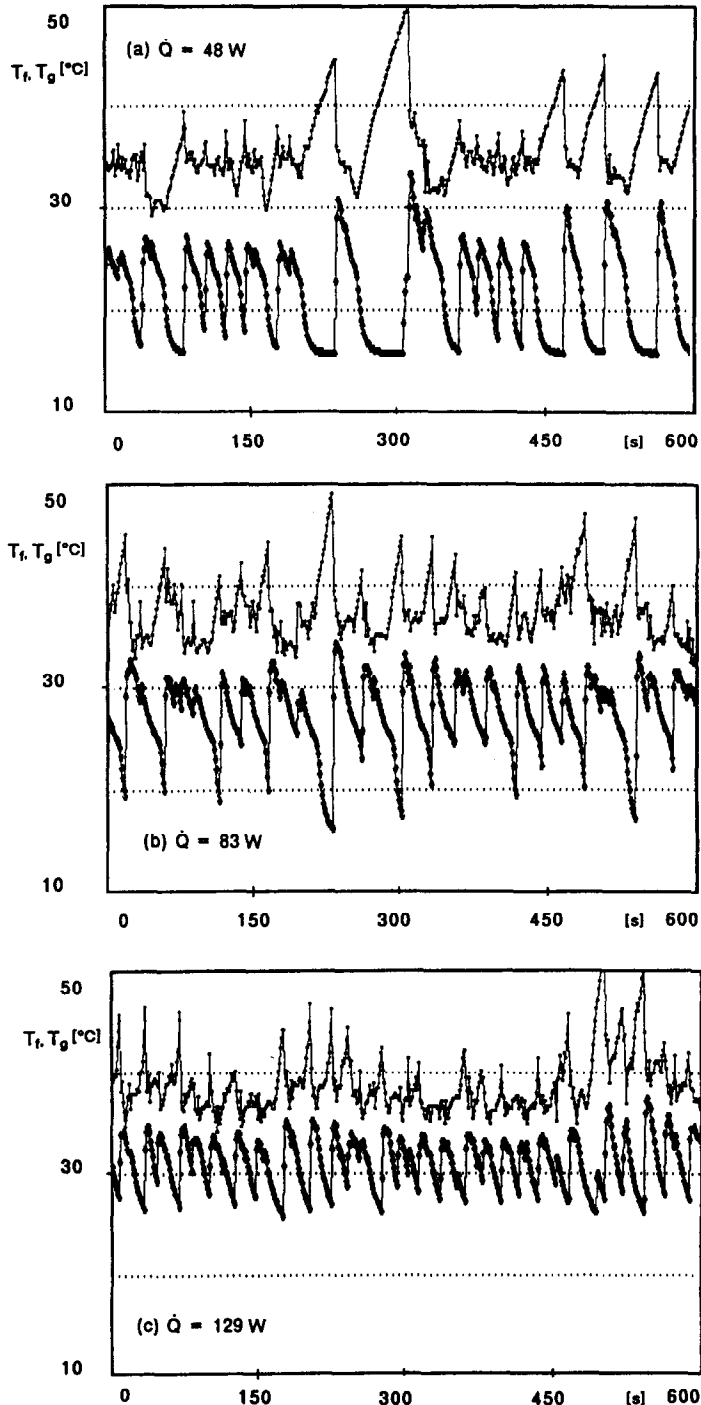

FIG. 3. Liquid and vapor temperatures in a transition between low-frequency boiling and fully-developed boiling. $D = 12$ mm; fluid, water; $p_r = 10^{-4}$.
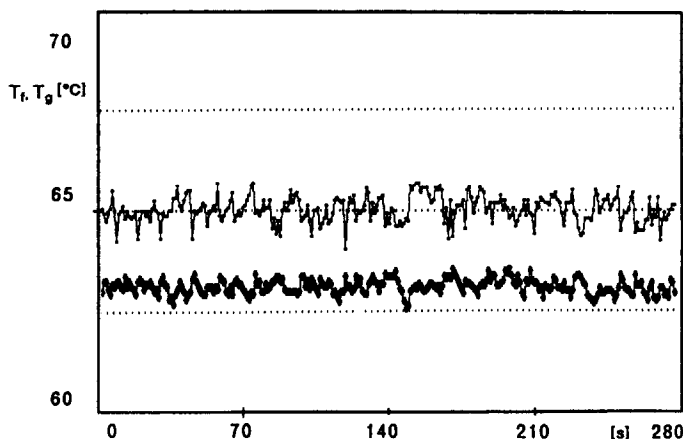
FIG. 4. Liquid and vapor temperatures in fully-developed boiling. $D = 12$ mm; fluid, water; $p_r = 10^{-3}$ and $\dot{Q} = 250$ W.

trend of liquid and vapor temperatures in fully-developed boiling is shown in Fig. 4. The temperatures still experience fluctuations, but these are restrained in 0.5°C for the liquid and 0.8°C for the vapor. These fluctuations, which remain also at high nucleation frequencies, are due to the intrinsically stochastic nature of boiling.

The thermosyphon operation is steady only 'on average', i.e. for a given pressure and power throughput, there is no single nucleation frequency, but a spectrum of frequencies which are related to phenomena such as stimulated nucleation and random operation decoupling. Thus, for each test we need to recognize a characteristic nucleation frequency. We conjecture that information about nucleation frequencies may be inferred by a spectral analysis of liquid or vapor temperatures. In this respect, we note that the vapor conditions are much more uniform than the liquid conditions and thus the vapor temperature is more suitable for this kind of analysis.

The estimate of the longer waiting times ($\tau_w \geqslant 10$ s), such as for the traces in Fig. 2, is carried out as follows. The waiting period starts when the measured vapor temperature begins to fall exponentially, i.e. when the evaporator and the condenser decouple. The waiting period ends when the vapor temperature, after falling below a low-threshold value predetermined for each run on the basis of a visual and a statistical analysis of the traces, has a jump greater than a threshold amplitude. When this occurs, a boiling burst couples the condenser to the evaporator again. The low-threshold temperature is chosen as the temperature below which the vapor stays for 63.2% of the test time. To estimate the shorter waiting times ($\tau_w < 10$ s but greater than or equal to 0.5 s that is the minimum significant time interval consistent with our sampling rate), such as for the traces in Fig. 3(c), only temperature oscillations of amplitude smaller than a threshold amplitude are considered, i.e. we do not consider the longer random operation decouplings. For each test, we determine the average
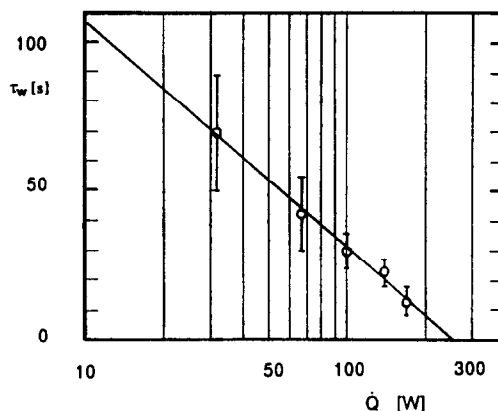

FIG. 5. Dependence of the average waiting time on power throughput. $D = 12$ mm; fluid, water; $p_r = 10^{-4}$, $\dot{Q}(0) = 250$ W, correlation coefficient $r = 0.996$.

value and the variance of the waiting time. Elimination–inclusion procedures have also been performed in order to minimize the variance.

Figure 5 shows the dependence of the average waiting times τ_w on power throughput $\dot{Q}$ in a semi-logarithmic scale; the graph refers to a given value of the pressure. Extrapolation of these data to zero waiting time yields a value of power throughput that we take as indicative of the minimum power needed at the given pressure for the onset of fully-developed boiling. The values of power throughput determined in this way are given in Table 1. The data show a strong dependence on $1/\sqrt{p'}$, specifically, the same functional dependence as our equation (16) for the intermittent/fully-developed-boiling frontier in the dynamic limit. Assuming that the variations of properties ρ_f, c_f and k_f with temperature are negligible between 20 and 80°C, if Δp^* is constant for all runs, then equation (16) may be written as

$$q_{wg_1} = G \frac{T^{0.25}}{\sqrt{p'}} \qquad (23)$$

Table 1. Data on intermittent/fully-developed-boiling frontier

p_r	T (°C)	T (K)	dp_s/dT (SI)	Ja†	Q (W)	q (W m^{-2})	$T^{0.25}/\sqrt{P'}$ (SI)	Notes
10^{-4}	19	292	138	508	250	3.316×10^4	0.351	D12–H$_2$O
10^{-4}	19	292	138	508	230	3.050×10^4	0.351	D12–H$_2$O
10^{-4}	19	292	138	508	500	2.653×10^4	0.351	D30–H$_2$O
3×10^{-4}	38	311	359	70	150	1.989×10^4	0.221	D12–H$_2$O
3×10^{-4}	38	311	359	70	400	2.122×10^4	0.221	D30–H$_2$O
10^{-3}	62	335	995	8	100	1.325×10^4	0.136	D12–H$_2$O
10^{-3}	62	335	995	8	200	1.061×10^4	0.136	D30–H$_2$O
5×10^{-3}	20	293	1033	3	100	1.325×10^4	0.129	D12 Acetone

† The Jakob numbers are estimated using the value $\Delta p = 670$ Pa.

where

$$G = \frac{\sqrt{\pi}(gk_f)^{1/3}(\rho_f c_f)^{5/12}\Delta p^{*0.75}}{2(c_{0.75}c_3)^{1/3}}$$

is a dimensional constant. As shown in Fig. 6, the experimental data correlate linearly with $T^{0.25}/\sqrt{p'}$ in a log–log plot, with a correlation coefficient $r = 0.976$ and a scatter less than or equal to 20%. For the constant G we find the value of $G = 89\,670$ (all variables in SI units). Therefore, the data seem to imply that Δp^* is approximately constant. Using the values $c_{0.75} = 2$ and $c_3 = 1.228$, as reported in the Appendix, and $G = 89\,670$ we find $\Delta p^* = 670$ Pa. Using this value we estimate the Jakob numbers given in Table 1. These values and the corresponding values of liquid superheat are lower than might be expected from standard boiling experiments at the same pressure. But our experimental conditions are different. Our geometry is quite constrained and, especially as we approach fully-developed boiling, the turbulence generated by the flow of other bubbles causes strong pressure fluctuations. As a result of these fluctuations, it is reasonable to expect that bubbles reach critical dimensions at much lower superheats than in standard experiments.

We can express this by writing

$$\Delta p^* = \frac{2\sigma}{R_c} - p_{g.ads} - p_{dist} \qquad (24)$$

where R_c is the mouth cavity radius (we assume a hemispherical critical nucleus with a radius equal to R_c as suggested by Griffith and Wallis [18]), $p_{g.ads}$ the pressure of the gas or vapor entrapped in the cavity and p_{dist} the amplitude of the liquid pressure fluctuations due to the detachment and the flow of other bubbles.

Figure 7 shows the experimental data and relations (16) and (17) on a $p'-q$ diagram. In equation (17) for the radius at detachment (static limit) R_{d_2} we used the value $R_{d_2} = 0.30$ mm taken from Kiper [19]. Equations (16) and (17) refer to the transition frontier in the dynamic and the static limit, respectively. The intersection point of these two limit solutions occurs for $Ja = \overline{Ja} \approx 7$. At that point the power is overestimated by 30% compared to that given by the complete solution (equation (15)); however, for $Ja < 18$ and $Ja > 4$ (i.e. for $p' < 700$ and $p' > 1400$) this error becomes less than 4%. Thus, the two limit solutions give a good approximation of the frontier between the intermittent and fully-developed boiling regimes.
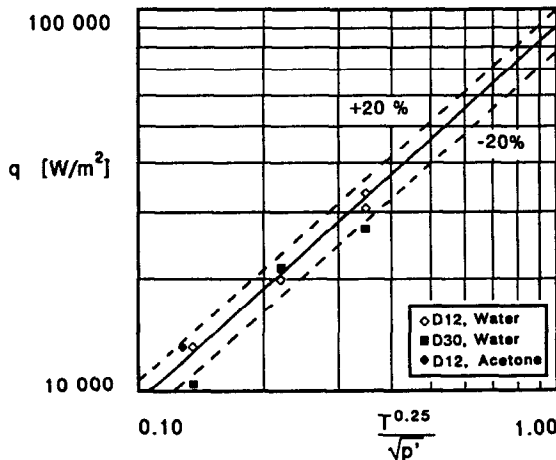

FIG. 6. Plot of experimental vs calculated thermal flux $q_{w_{fi}}$ at the transition frontier between intermittent and fully-developed boiling.
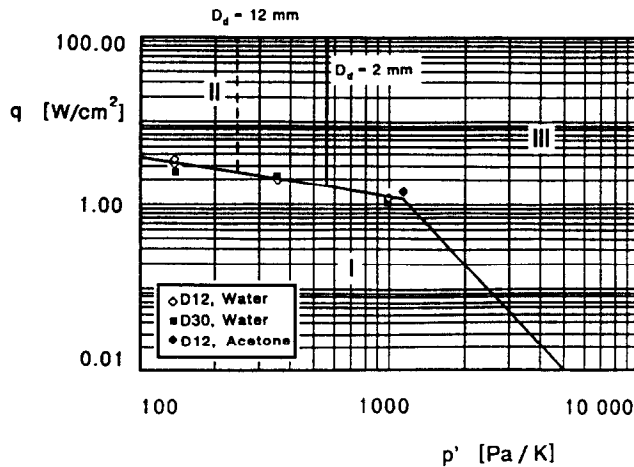
FIG. 7. Frontiers between the main boiling regimes: (I) intermittent boiling; (II) slug-fully-developed boiling; (III) bubble-fully-developed boiling.

Equation (22) is also plotted in Fig. 7 for two bubble diameters, i.e. $D_d = 2$ and 12 mm, that satisfy respectively the two criteria $D_d/D \ll 1$ and $D_d/D \sim 1$ for $D = 12$ mm. The location of the $D_d/D \sim 1$ boundary (dotted line) is only qualitative because it is obviously inconsistent with the assumption $D_d/D \ll 1$ used in deriving the equation for the detachment diameter D_d.

In summary, three regions are defined in the $p'-q$ plane shown in Fig. 7. In region I we have intermittent boiling (the further we operate from the frontier the lower is the nucleation frequency). In region II we have fully-developed boiling, but the bubbles have dimensions comparable to the device dimension (slug-fully-developed-boiling regime). In region III we have bubble-fully-developed boiling, characterized by thick jets of small bubbles. It is noteworthy that the right-hand branch of the frontier cannot be extended indefinitely to low thermal fluxes, because eventually it crosses the frontier, not plotted, between boiling and natural convection. Of course, the three regions are bounded in the upper part by a fourth region, not plotted, where the thermosyphon cannot operate due to the onset of some critical condition or operating limit as flooding. Finally, the $p'-q$ plane is perfectly equivalent to a $p-q$ or p_r-q plane, since the saturation pressure is a monotonic and convex function of temperature. Here, we have chosen the variable p' rather than p so as to avoid empirical or numerical relations in equations (16), (17) and (22).

6. CONCLUSIONS

Especially at low pressures, the performance of a closed two-phase thermosyphon with medium and large filling is characterized by unsteady operation. Our analysis and experimental data show that the reason for such unsteady operation is to be found in the boiling mechanisms. Boiling may occur with a wide spectrum of different nucleation frequencies and bubble dimensions depending on liquid superheat, vapor density and other thermodynamic properties.

We classify the boiling regimes on the basis of the frequency of bubble nucleation and the ratio of bubble diameter to device diameter. A criterion for the inter-mittent/fully-developed-boiling frontier is based on the ratio of the bubble-nucleation waiting time and the bubble growth time. From this criterion we obtain a correlation between power throughput, working-fluid pressure and nucleation critical superheat (equation (15)). This correlation explains the known empirical observation that intermittent boiling regimes are related to low operating pressures. A correlation for slug/bubble-boiling frontier is also derived (equation (22)).

An experimental analysis performed on transparent devices using mainly water as the working fluid yields the dependence of nucleation frequencies on power throughput and operating pressure. The data are in good agreement with the proposed correlation in the dynamic limit (equation (16) or (23)) for the frontier between intermittent boiling and fully-developed boiling except for the constant G which is evaluated experimentally. More data spanning a broader range of operating conditions and including measurements of local superheat, are needed to further validate our theoretical considerations. Also, data on bubble growth in constrained geometries are needed in order to better determine the bubble dimensions at detachment and extend the validity of our results. Finally, work is needed to evaluate the usefulness of power spectrum analyses and phase-plane analyses to better characterize the bubble nucleation frequency.

REFERENCES

1. H. Imura, H. Sasaguchi and H. Kozai, Critical heat flux in a closed two-phase thermosyphon. *Int. J. Heat Mass Transfer* **26**, 1181–1188 (1983).
2. F. Dobran, Steady-state characteristics and stability thresholds of a closed two-phase thermosyphon, *Int. J. Heat Mass Transfer* **28**, 949–957 (1985).
3. J. G. Reed and C. L. Tien, Modeling of the two phase closed thermosyphon, *ASME J. Heat Transfer* **109**, 722 (1987).
4. B. S. Larkin, An experimental study of two-phase thermosyphon tube, *Trans. Can. Soc. Mech. Engng* **14**, 17–24 (1971).
5. M. K. Bezrodnyi and D. V. Elekseyenko, Boiling heat transfer in a closed two-phase thermosyphon, *Heat Transfer—Sov. Res.* **9**, 14–20 (1977).
6. T. Fukano, K. Kadoguchi and C. L. Tien, Oscillation phenomena and operating limits of the closed two-phase thermosyphon, *Proc. 8th IHTC*, Vol. 5, pp. 2325–2330 (1987).
7. C. Casarosa, E. Latrofa and A. Shelginski, The geyser effect in a two-phase closed thermosyphon, *Int. J. Heat Mass Transfer* **26**, 933–941 (1983).
8. Y. Y. Hsu, On the size range of the active nucleation cavities on a heating surface, *ASME J. Heat Transfer* **84**, 207 (1962).
9. C. Y. Han and P. Griffith, The mechanism of heat transfer in nucleate pool boiling—1. Bubble initiation, growth and departure, *Int. J. Heat Mass Transfer* **8**, 887–904 (1965).
10. A. Niro, A study of closed two-phase thermosyphons, Doctoral Thesis, Politecnico di Milano, Milano, Italy (1987).
11. J. S. Saini, C. P. Gupta and S. Lal, Effect of Jakob number on forces controlling bubble departure in nucleate bubble boiling, *Int. J. Heat Mass Transfer* **18**, 472–474 (1975).
12. A. P. Hatton, D. D. James and T. L. Liew, Measurement of bubble characteristics for pool boiling from single cylindrical cavities. In *Heat Transfer 1970*. Elsevier, New York (1970).
13. C. P. Witze, V. E. Schrock and P. L. Chambré, Flow about a growing sphere in contact with plane surface, *Int. J. Heat Mass Transfer* **11**, 1637–1652 (1968).
14. B. B. Mikic, W. M. Rohsenow and P. Griffith, On bubble growth rates, *Int. J. Heat Mass Transfer* **13**, 657–666 (1970).
15. S. J. D. Van Stralen, R. Cole, W. M. Sluyter and M. S. Sohal, Bubble growth rates in nucleate boiling of water at subatmospheric pressures, *Int. J. Heat Mass Transfer* **18**, 655–669 (1975).
16. W. Zijl, F. J. M. Ramakers and S. J. D. Van Stralen, Global numerical solutions of growth and departure of a vapor bubble at a horizontal superheated wall in a pure liquid and a binary mixture, *Int. J. Heat Mass Transfer* **22**, 401–420 (1979).
17. R. Cole and H. L. Shulman, Bubble growth at high Jakob numbers, *Int. J. Heat Mass Transfer* **9**, 1377–1390 (1966).
18. P. Griffith and J. D. Wallis, The role of surface conditions in nucleate boiling, *Chem. Engng Prog. Symp. Ser.* **56**, 49 (1960).
19. A. M. Kiper, Minimum bubble departure diameter in nucleate pool boiling, *Int. J. Heat Mass Transfer* **14**, 931–937 (1971).
20. J. K. Stewart and R. Cole, Bubble growth rates during nucleate boiling at high Jakob numbers, *Int. J. Heat Mass Transfer* **15**, 655–663 (1972).
21. S. J. D. Van Stralen, M. S. Sohal, R. Cole and W. M. Sluyter, Bubble growth rate in pure and binary systems: combined effect of relaxation and evaporation microlayers, *Int. J. Heat Mass Transfer* **18**, 453–467 (1975).

APPENDIX

During bubble growth, the vapor pressure is related to the motion of the liquid–vapor interface and the mass and energy flux through it. For a spherical bubble growing on a surface in a uniformly superheated liquid at temperature T_{f_x} and pressure p_f, the momentum and energy equations are

$$4(R\ddot{R}+\dot{R}^2)\ln\left(\frac{R}{R_0}\right)\cos^2\frac{\Phi}{2}+4R^2\cos^2\frac{\Phi}{2}=\frac{p_g-p_f}{\rho_f}-\frac{2\sigma}{\rho_f R} \tag{A1}$$

$$T_{f_x}-T_g=\frac{\rho_g h_{fg}}{k_f}R\sqrt{(\pi at)}. \tag{A2}$$

Equation (A1) is that derived by Witze *et al.* [13] for inviscid and irrotational flow. Unlike the case of bubble growth in infinite geometry, the vapor pressure depends on the angle at center Φ and has a maximum at the bubble top ($\Phi = 0$). The vapor, for its high diffusivity, may be assumed to be at saturation conditions, i.e. $p_g = p_s(T_g)$. Assuming

$$\frac{2\sigma}{p_f R}\ll 1 \tag{A3}$$

the right-hand side of equation (A1) may be simplified to

$$\text{RHS}=\frac{p_g-p_f}{\rho_f}$$

or, equivalently

$$\text{RHS}=\frac{1}{\rho_f}[p_s(T_{f_x})-p_f]\left(1-\frac{p_s(T_{f_x})-p_g}{p_s(T_{f_x})-p_f}\right)$$

$$=\frac{\Delta p^*}{\rho_f}\left(1-\frac{T_{f_x}-T_g}{T_{f_x}-T_s(p_f)}\right).$$

Moreover, neglecting the inertial terms, i.e. assuming

$$\frac{4(R\ddot{R}+\dot{R}^2)\ln(R/R_0)\cos^2(\Phi/2)+4\dot{R}^2\cos^2(\Phi/2)}{\Delta p^*/\rho_f}\ll 1. \tag{A4}$$

Equation (A1) becomes

$$\frac{T_{f_x}-T_g}{T_{f_x}-T_s(p_f)}\approx 1. \tag{A1'}$$

Thus, bubble growth is controlled only by the energy equation, i.e.

$$T_{f_x}-T_s(p_f)=\frac{\rho_g h_{fg}}{k_f}\dot{R}\sqrt{(\pi at)} \tag{A2'}$$

which yields equation (9′) where $\theta = T_{f_x}-T_s(p_f)$. Using equation (9′), conditions (A3) and (A4) become

$$\frac{2\sigma}{\rho_f c\,Ja\,\sqrt{(at)}}+\frac{2\sigma}{\rho_f c\,Ja\,\sqrt{(a\tau_g(t/\tau_g))}}\ll 1 \tag{A3'}$$

$$\frac{c^2\,Ja^2(a/t)}{\Delta p^*/\rho_f}+\frac{c^2\,Ja^2(a/\tau_g)}{(t/\tau_g)\Delta p^*/\rho_f}\ll 1. \tag{A4'}$$

Assuming that conditions (A3′) and (A4′) hold at the beginning of bubble growth, i.e. for $t \ll \tau_g$, and using equation (12) for τ_g we obtain

$$p_f\gg\frac{2\sigma}{\dfrac{t}{\tau_g}\left(\dfrac{3\sigma R_s\sin\Phi}{2\rho_f g}\right)^{1/3}}\approx 2000\text{ Pa} \tag{A3''}$$

$$Ja\ll\left(\frac{1}{c^2 a^2}\left(\frac{3\sigma R_s\sin\Phi}{2\rho_f g}\right)^{2/3}\frac{\Delta p^*}{\rho_f}\frac{t}{\tau_g}\right)^{1/4}\approx 25 \tag{A4''}$$

where we used the values $c_1 = 1.5$ and $R_{d_s}=(3\sigma R_s \times\sin\Phi/2\rho_f g)^{1/3}=0.3$ mm taken from the literature [15, 19]. Condition (A3″) is satisfied in most situations. Thus, con-
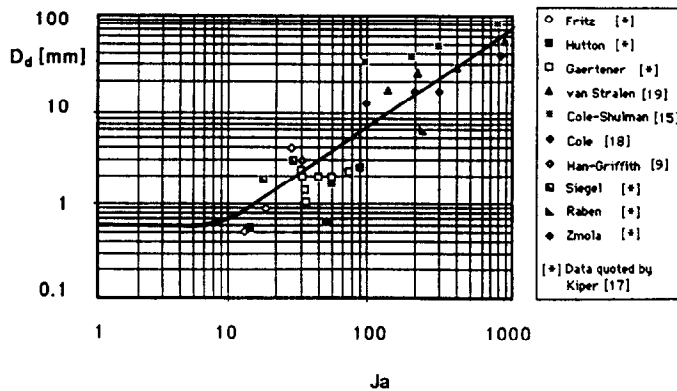
FIG. A1. Plot of equation (20) and experimental data taken from the literature.

dition (A4″) implies that the 'diffusive' solution (equation (9′)) is valid for $Ja \leqslant 3$. A large collection of data taken from the literature [9, 12, 17, 19, 20, 21] show good agreement with the empirical solution (9″) for $Ja \geqslant 10$ provided we take $c_{0.75} = 2$. The constant c_3 may be obtained by a best fit of equation (20) on the same experimental data. Since the largest error made using equation (20′) (dynamic limit) to calculate the detachment diameter instead of equation (20) (general solution) for $Ja \geqslant \widetilde{Ja}$ is less than 25%, it is simpler

to use equation (20′), i.e.

$$R_{d_1} = c_m^{4/3} c_3^{1/3} \left(\frac{a^2}{g}\right)^{1/3} Ja^{(4.3)m}. \tag{A5}$$

Thus, we get $c_3 = 1.228$. Figure A1 shows the literature data and equation (20) plotted using the values for constants $c_{0.75}$, c_3 and D_{d_1} as reported above.

REGIMES D'EBULLITION DANS UN THERMOSIPHON DIPHASIQUE FERME

Résumé—Des résultats expérimentaux et un modèle analytique sur les mécanismes d'ébullition dans un thermosiphon diphasique fermé sont présentés pour définir les frontières entre les régimes principaux d'ébullition et, en particulier, la frontière entre ébullition intermittante et ébullition pleinement développée. Les régimes d'ébullition sont classés sur la base des fréquences de nucléation de bulles. Un critère pour la frontière signalée plus haut est basé sur le rapport du temps d'attente de la nucléation au temps de croissance de la bulle. A partir de ce critère, on obtient une relation entre la puissance fournie, la pression du fluide de travail et la surchauffe critique de nucléation. Des données expérimentales sur les conditions opératoires, les températures et les fréquences de nucléation ont la même dépendance fonctionnelle que pour la relation proposée.

SIEDEBEREICHE IN EINEM GESCHLOSSENEN ZWEIPHASENTHERMOSYPHON

Zusammenfassung—Es werden experimentelle Ergebnisse und ein analytisches Modell für den Siedemechanismus in einem geschlossenen Zweiphasenthermosyphon vorgestellt, um die Fronten zwischen den Hauptsiedebereichen und—insbesondere—die Front zwischen dem intermittierenden und dem voll entwickelten Sieden zu beschreiben. Die Siedebereiche werden klassifiziert auf der Grundlage der Frequenz der Blasenbildung und des Verhältnisses zwischen Blasendurchmesser und Rohrdurchmesser. Ein Kriterium für die Grenze zwischen dem intermittierenden und dem voll entwickelten Sieden beruht auf dem Verhältnis zwischen der Wartezeit bei der Blasenbildung und der Wachstumszeit. Aus diesem Kriterium ergibt sich eine Korrelation zwischen dem transportierten Wärmestrom, dem Druck des Arbeitsstoffes und der Überhitzung beim Sieden. Meßdaten für die Betriebsbedingungen, die Temperaturen und die Frequenzen der Blasenbildung zeigen die gleiche funktionale Abhängigkeit wie die vorgeschlagene Korrelation.

РЕЖИМЫ КИПЕНИЯ В ЗАМКНУТОМ ДВУХФАЗНОМ ТЕРМОСИФОНЕ

Аннотация—Представлены экспериментальные результаты и аналитическая модель механизмов кипения в замкнутом двухфазном термосифоне с целью определения границ между основными режимами кипения, в частности, между прерывистым и полностью развитым кипением. Режимы кипения классифицируются на основе частоты образования пузырьков и отношения их диаметра к диаметру устройства. Критерий границы между прерывистым и установившимся кипением базируется на отношении времени ожидания к времени роста. По данному критерию получены зависимости между пропускной мощностью, давлением рабочей жидкости и критическим перегревом при образовании пузырьков. Функциональная зависимость экспериментальных данных по режимным параметрам, температурам и частотам образования пузырьков идентична предложенному соотношению.